

Mesonic exchange currents and radiative thermal neutron capture by the deuteron

J. Torre

Institut des Sciences Nucléaires, 38026, Grenoble CEDEX, France

B. Goulard

Laboratoire de Physique Nucléaire, Université de Montréal, Montréal, Québec, Canada H3C 3J7

(Received 10 January 1983)

Radiative capture of thermal neutrons by the deuteron: $n+d \rightarrow {}^3\text{H} + \gamma$ is investigated. Wave functions built upon definite nucleon-nucleon forces are used to describe both the bound state and the scattering two-body state. The role of mesonic exchange currents and of two-nucleon forces are investigated in detail. Finally, the bearing of genuine three-nucleon forces on the cross sections and other related properties is exhibited.

[NUCLEAR REACTIONS Triton. Radiative neutron capture. Mesonic exchange currents. $M1$ transition. Three-body forces.]

I. INTRODUCTION

Investigations on mesonic exchange currents (MEC's) in $A > 4$ nuclei very often lead to conclusions somewhat obscured by standard nuclear structure uncertainties. From this point of view, three-nucleon systems constitute a rather privileged laboratory since, although they do not display the simplicity of two-nucleon systems, a rather clear link between nucleon interactions and the resulting (bound and unbound) states has been established^{1,2}; besides, many-body features, precursors of physics in heavier nuclei, are already showing up at that stage. Indeed, pioneering^{3,4}—and soft pioneering⁵—work MEC's in nuclei mostly came up in relation to $A = 3$ nuclei, such as ${}^3\text{H}$ beta decay and ${}^3\text{He}$ and ${}^3\text{H}$ magnetic moments.

As a consequence of the difficulty of tackling three-body dynamics in the continuum, the search for reactions involving unbound states has come up more recently.² In view of the very recent availability of unbound deuteron-neutron zero energy states built on the basis of realistic nucleon-nucleon interaction, more refined estimates of the radiative capture of thermal neutrons by the deuteron, $n+d \rightarrow {}^3\text{H} + \gamma$, are possible. The calculation of this process cross section—comparable in accuracy with already achieved calculations for the corresponding process $n+p \rightarrow d + \gamma$, and incorporating MEC's—is the object of this work. As the work goes along, the interplay between nuclear forces, correlation functions, MEC's, and binding energies will be unfolded as much as possible.

A few words are in order to show the interest of such an investigation. The successful treatment of the similar reaction $n+p \rightarrow d + \gamma$ induced investigators of weak and electromagnetic nuclear currents to take MEC's more seriously.⁶ Specifically, while cross sections calculated in the nucleons only impulse approximation (NOIA) framework (302.5 ± 4.0 mb) could not match experimental data (334.2 ± 0.5 mb), inclusion of MEC's brought up the missing 30 mb up to a surprising accuracy. In view of the various mesonic exchange contributions to be presented in the following, it is worthwhile to review the currently accepted explanation of such a satisfactory situation. The first point is the power of low energy theorems for diagrams involving one pion [see Fig. 1(a)]. Out of the three

main diagrams displayed in Figs. 2(a)–(c), two are essentially based on soft pion theorems, and, hence, are rather model independent. These are the pionic and pair diagrams yielding 66% (6.6%) of the MEC (total) contribution. The third diagram, 2(c), involving an intermediate Δ state, does not involve a soft pion and is very sensitive to the D state component of the deuteron. In other words, it spoils the “nice” soft pion picture but is not that significant for the overall cross section. Second, two-nucleon correlation functions are very small for the short nucleon interdistances; in that short-range region, besides pion currents, the mesonic operators implying heavier (shorter Compton wavelength) mesons (ρ, ω, \dots) are also at work. In these conditions, the corresponding transition matrix elements built up from a short-range operator bracketed by depressed short-range states yield negligible contributions; however, this argument, partly because of the imperfect knowledge of what really happens in the short-range nucleon-nucleon region, keeps a qualitative flavor.

A similar reaction is the radiative thermal neutron absorption by a deuteron leading to the triton $n+d \rightarrow {}^3\text{H} + \gamma$. Such a reaction also proceeds through an $M1$ transition from the unbound ${}^2S_{1/2}$ and ${}^4S_{3/2}$ neutron-deuteron states to the bound triton described by the usual mixture of the space symmetry S component ($\approx 90\%$) and mixed symmetry S' component ($\approx 1\%$), together with the D component ($\approx 9\%$). The original feature of this reaction is a drastic quenching of the calculated NOIA transition matrix element. It happens that the bound S component does not participate in the $M1$ transition on the basis of its quasiorthogonality to the unbound states; hence, the reac-

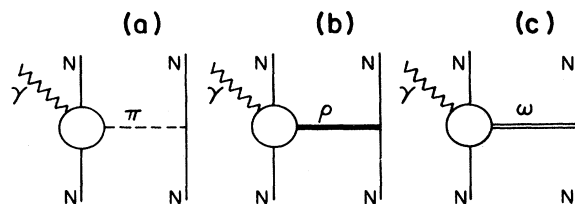


FIG. 1. Diagrams with γNN vertex unspecified and $M = \pi, \rho, \omega$.

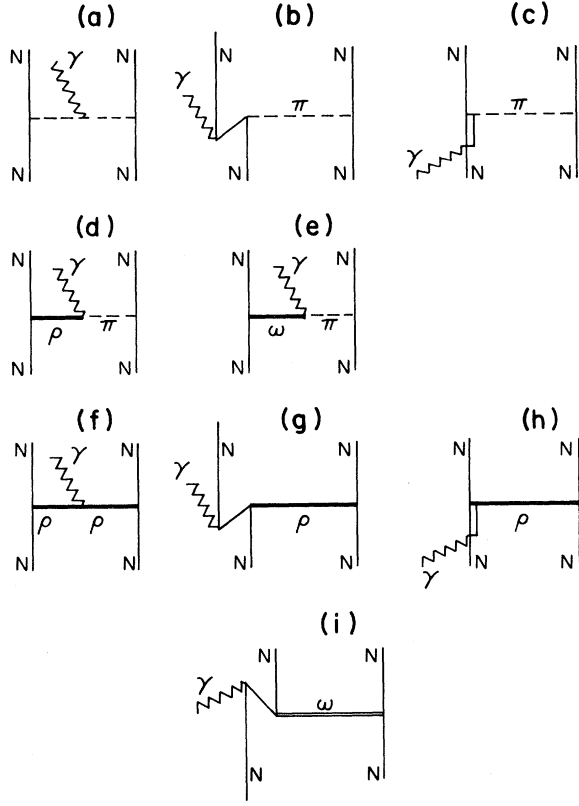


FIG. 2. Detailed diagrams considered in the main text.

tion is severely hindered and MEC's are expected to be quite significant. Indeed, a calculation by Hadjimichael,⁷ using approximate wave functions and a microscopic treatment of MEC's, has reflected these features quite

clearly with a 50% MEC contribution, so bringing the NOIA result (≈ 3 mb) closer to the experimental data ($\approx 0.5-0.6$ mb).⁸

For these reasons, a consistent treatment of the three nucleon wave function and its interplay with the various possible MEC's is quite crucial. It is expected that incorporation of Grenoble three nucleon states, built up with the same nucleon-nucleon realistic interaction for both bound and unbound states, will ensure a maximal self-consistency to the forthcoming calculations. Thus, the $M1$ one- and two-body operators will be briefly described in Sec. II and Grenoble three nucleon states conventions will be recalled; the recent incorporation of genuine three-body forces by this latter group will be briefly described. Some results on static magnetic moments will be given in Sec. III. After a brief description of the expressions relevant to the radiative cross section, the bearing of nucleon-nucleon forces on these cross sections will be first scrutinized in the NOIA framework, then the role of MEC contributions will be demonstrated. A conclusion will follow.

II. MESONIC EXCHANGE OPERATORS

Besides the single-particle operators which take the well known expression

$$\vec{M}^{[1]} = \frac{e\hbar}{2m_N} \sum_{j=1}^3 \left[\left[\frac{1}{2}(1+\tau_j^z)\mu_p\vec{\sigma}_j + \frac{1}{2}(1+\tau_j^z)\mu_n\vec{\sigma}_j \right] + \left[\frac{1+\tau_j^z}{2} \vec{1}_j \right] \right] \quad (1)$$

with m_N the nucleon mass, $\mu_p = 2.793 \mu_N$ and $\mu_n = 1.913 \mu_N$ the nucleon magnetic moments, the MEC's are written following the standard expressions^{4,5}:

$$\vec{M}^{[2]} = \sum_{j,k=1}^3 \vec{M}_{jk}^v = \frac{1}{2} \frac{e\hbar}{2m_N} \{ (\vec{\tau}_j \times \vec{\tau}_k)^z [(\vec{\sigma}_j \times \vec{\sigma}_k)g_{I} + T_{jk}^{(\times)}g_{II}] + (\vec{\tau}_j - \vec{\tau}_k)^z [(\vec{\sigma}_j - \vec{\sigma}_k)h_{I} + T_{jk}^{(-)}h_{II}] + (\vec{\tau}_j + \vec{\tau}_k)^z [(\vec{\sigma}_j + \vec{\sigma}_k)j_{I} + T_{jk}^{(+)}j_{II}] \}, \quad (2)$$

$$\vec{M}^{S,[2]} = \sum_{j,k=1}^3 \vec{M}_{jk}^S = \frac{1}{2} \frac{e\hbar}{2m_N} \{ (\vec{\sigma}_j + \vec{\sigma}_k)l_{I} + T^{(+)}l_{II} + \tau_j^z\tau_k^z [(\vec{\sigma}_j + \vec{\sigma}_k)k_{I} + T_{jk}^{(+)}k_{II}] + \vec{\tau}_j \cdot \vec{\tau}_k [(\vec{\sigma}_j + \vec{\sigma}_k)m_{I} + T_{jk}^{(+)}m_{II}] \};$$

$$T_{jk}^{(x)} = (\vec{\sigma}_j \times \vec{\sigma}_k) \cdot \hat{r}_{jk} \hat{r}_{jk} - \frac{1}{3} (\vec{\sigma}_j \times \vec{\sigma}_k), \quad x = +, -, \times. \quad (3)$$

The functions $g_{I,II}$, $h_{I,II}$, $j_{I,II}$, $k_{I,II}$, $l_{I,II}$, and $m_{I,II}$, listed in Refs. 5 and 9, will be given later on for the various relevant diagrams.

"Translationally noninvariant operators" have been excluded because their contribution to the static moments is small, the orbital motion being essentially in an s state. Furthermore, contributions to recoil and wave function renormalization have been omitted. On the other hand, since we hold a good amount of confidence in the short-range part of our two-nucleon correlation functions, it is worthwhile to use an exhaustive list of diagrams implying pions as carriers of the nucleon-nucleon interaction, and also heavier mesons such as ρ and ω .

This is why, in Fig. 1, the three following exchange processes selected as relevant between nucleons j and k are displayed. Each of these processes (involving, successively, π , ρ , and ω bosons) is described in terms of the specific diagrams listed in Fig. 2.

To calculate those diagrams in terms of the radial functions written in Eqs. (2) and (3), the following equalities are to

be used, together with the conventions and numerical values given after the presentations of the two-body sequence: π -meson current [Fig. 2(a)]:

$$g_I(x) = -\frac{2}{3} \frac{m_N}{m_\pi} (2-x_\pi) Y_0(x_\pi), \quad g_{II}(x) = -\frac{m_N}{m_\pi} f_{\pi NN}^2 Y_1(x_\pi);$$

π -pair excitation current [Fig. 2(b)]:

$$g_I(x) = -\frac{2}{3} g_{II}(x) = \frac{2}{3} \frac{m_N}{M_\pi} f_{\pi NN}^2 Y_1(x_\pi);$$

N^* - π current [Fig. 2(c)]:

$$g_I(x) = \frac{4}{9} \frac{1}{2} (\mu_\rho - \mu_n) h_1(0) m_\pi^3 Y_0(x_\pi), \quad g_{II}(x) = -\frac{6}{9} \frac{1}{2} (\mu_\rho - \mu_n) h_1(0) m_\pi^3 Y_2(x_\pi),$$

$$h_I(x) = j_I(x) = -\frac{1}{9} \frac{1}{2} (\mu_\rho - \mu_n) 4h_2(0) m_\pi^3 Y_0(x_\pi), \quad h_{II}(x) = j_{II}(x) = -\frac{3}{9} \frac{1}{2} (\mu_\rho - \mu_n) 4h_2(0) m_\pi^3 Y_2(x_\pi).$$

The following are the diagrams implying one ρ exchange contribution.

ρ -meson excitation current [Fig. 2(f)]:

$$g_I(x) = -\frac{4}{3} \frac{m_N}{m_\rho} f_{\rho NN}^2 (1+K_v)^2 (1+\frac{1}{2}\kappa_\rho)(x_\rho-2) Y_0(x_\rho), \quad g_{II}(x) = -\frac{m_N}{m_\rho} f_{\rho NN}^2 (1+K_v)^2 (1+2\kappa_\rho) Y_1(x_\rho);$$

ρ -pair current [Fig. 2(g)]:

$$g_I(x) = -\frac{2}{3} g_{II}(x) = \frac{4}{3} h_{II}(x) = \frac{2}{3} \frac{m_N}{m_\rho} f_{\rho NN}^2 (1+K_v)^2 Y_1(x_\rho), \quad h_I(x) = -\frac{1}{3} \frac{m_N}{m_\rho} f_{\rho NN}^2 [(1+2K_v)(1+x_\rho)+6] Y_0(x_\rho),$$

$$j_I(x) = \frac{1}{2} m_I(x) = \frac{1}{3} \frac{m_N}{m_\rho} f_{\rho NN}^2 (5-2K_\rho) Y_0(x_\rho), \quad j_{II}(x) = \frac{1}{2} m_{II}(x) = \frac{1}{2} \frac{m_N}{m_\rho} f_{\rho NN}^2 (1+K_v^2) Y_1(x_\rho);$$

N^* - ρ current [Fig. 2(h)]:

$$g_I(x) = h_I(x) = -j_I(x) = \frac{64}{75} (\mu_\rho - \mu_n) \frac{m_\rho}{m_{N^*} - m_N} f_{\rho NN}^2 (1+K_v)^2 Y_0(x_\rho),$$

$$g_{II}(x) = \frac{1}{2} h_{II}(x) = \frac{1}{2} j_{II}(x) = \frac{16}{25} (\mu_\rho - \mu_n) \frac{m_\rho}{m_{N^*} - m_N} f_{\rho NN}^2 (1+K_v)^2 Y_2(x_\rho).$$

The following are the diagrams implying one ω exchange.

ω -pair current [Fig. 2(i)]:

$$h_I(x) = \frac{1}{3} \frac{m_N}{m_\omega} f_{\omega NN}^2 [(1+2K_s)(x_\omega+1)+6] Y_0(x_\omega), \quad j_I(x) = \frac{1}{2} h_I(x) = \frac{1}{3} \frac{m_N}{m_\omega} f_{\omega NN}^2 (5-x_\omega) Y_0(x_\omega),$$

$$h_{II}(x) = -\frac{1}{2} \frac{m_N}{m_\omega} f_{\omega NN}^2 (1+K_s)^2 Y_1(x_\omega), \quad j_{II}(x) = \frac{1}{2} I_{II}(x) = \frac{1}{2} \frac{m_N}{m_\omega} f_{\omega NN}^2 (1+K_s^2) Y_1(x_\omega).$$

Terms implying ρ - ω [Fig. 2(d)] and ω - π diagrams [Fig. 2(e)] correspond to

$$m_I(x) = 2\xi_\rho \frac{m_\pi^3}{m_\rho(m_\rho^2 - m_\pi^2)} \left[Y_0(x_\pi) - \left(\frac{m_\rho}{m_\pi} \right)^3 Y_0(x_\rho) \right],$$

$$m_{II}(x) = 6\xi_\rho \frac{m_\pi^3}{m_\rho(m_\rho^2 - m_\pi^2)} \left[Y_2(x_\pi) - \left(\frac{m_\rho}{m_\pi} \right)^3 Y_2(x_\rho) \right],$$

and

$$h_I(x) = \xi_\omega \frac{m_\pi^3}{m_\omega(m_\omega^2 - m_\pi^2)} \left[Y_0(x_\pi) - \left(\frac{m_\omega}{m_\pi} \right)^3 Y_0(x_\omega) \right],$$

$$h_{II}(x) = 3\xi_\omega \frac{m_\pi^3}{m_\omega(m_\omega^2 - m_\pi^2)} \left[Y_2(x_\pi) - \left(\frac{m_\omega}{m_\pi} \right)^3 Y_2(x_\omega) \right].$$

In these various contributions, several expressions take the following values⁹:

masses:

$$m_\rho = 933.28 \text{ MeV}, \quad m_N = 939.57 \text{ MeV},$$

$$m_N = 938.9 \text{ MeV}, \quad m_{N^*} = 1232 \text{ MeV},$$

$$m_{\pi^\pm} = 139.57 \text{ MeV}, \quad m_\rho = 776 \text{ MeV},$$

$$m_\omega = 872.6 \text{ MeV};$$

magnetic moments:

$$\mu_p = 2.7928, \quad \mu_n = -1.9130;$$

$$\mu_v = 3.706, \quad \mu_s = -0.1202, \quad \mu_p = 0.1;$$

$$\kappa_\rho = 0.14, \quad K_v = 6.6;$$

$$K_s = -0.12;$$

coupling constants:

$$g_{\pi NN} = 13.49;$$

$$g_{\rho NN}=2.84, \quad g_{\rho\pi\gamma}=0.406,$$

$$g_{\omega NN}=7.60, \quad g_{\omega\pi\gamma}=2.03;$$

being at essentially $q \approx 0$ transfer, the meson-baryon vertices are taken to be constant;

radial functions:

$$x_B = \frac{m_B}{\hbar c} x,$$

$$Y_0(x) = e^{-x}/x, \quad Y_1(x) = (1+x)Y_0(x),$$

$$Y_2(x) = \left(1 + \frac{3}{x} + \frac{3}{x^2}\right) Y_0(x).$$

III. WAVE FUNCTIONS

Several wave functions are available for bound states and unbound states as well. In the present work, the wave functions used are "exact" solutions of the Faddeev equations for the three-nucleon interaction via a local interac-

tion both for the ground state and the zero energy neutron-deuteron state. Practical solutions for three-nucleon bound states and nonzero energy neutron-deuteron states have now been available for some time; however, the availability of such solutions for the zero energy neutron-deuteron states in the same framework is more recent.² It is here recalled that the wave function $\phi_{MT_Z}^{JT}(\vec{x}, \vec{y})$, where (\vec{x}, \vec{y}) is in the three-nucleon center of mass system coordinates, is related to the $(\vec{r}_1, \vec{r}_2, \text{ and } \vec{r}_3)$ coordinates in some frame by the transformation

$$\begin{pmatrix} \vec{r}_1 \\ \vec{r}_2 \\ \vec{r}_3 \end{pmatrix} = \begin{pmatrix} 1 & -1 & 0 \\ 1 & \frac{1}{2} & \frac{1}{2} \\ 1 & \frac{1}{2} & -\frac{1}{2} \end{pmatrix} \begin{pmatrix} 0 \\ \vec{y}/\sqrt{3} \\ \vec{x} \end{pmatrix};$$

also, $\Phi_{MT_Z}^{JT}(\vec{x}, \vec{y})$ is written as a sum over the various components characterized by orbital, spin, and total angular momenta $(\lambda, \frac{1}{2}, \text{ and } j)$ of particle 1 and $(l\sigma J)$ of particles 2 and 3, combining to yield the total angular momentum $[J, M]$ and isospin $[T, T_Z]$,

$$\Phi_{MT_Z}^{JT}(\vec{x}, \vec{y}) = \sum_{\lambda\sigma j l \sigma J} \frac{1}{x y} \phi_{\lambda l \sigma}^{j(1/2)(1/2)}(x, y) [\mathcal{Y}_{\lambda(1/2)}^j(\hat{y}) \otimes \mathcal{Y}_{l\sigma}^J(\hat{x})] \eta_{(1/2)T}^{TT_Z}, \quad (4)$$

where antisymmetry of the wave function in the interchange of particles 2 and 3 requires that $l + \sigma + \tau$ be odd. Three realistic nucleon-nucleon forces are considered to follow the effects of an increasing tensor contribution in the even triplet subspace, i.e., the MT 13 force with no tensor force and then no D state,¹⁰ the Sprung-de Tourreil supersoft core type c (SSCc),¹¹ and the Reid soft core (RSC).¹² Furthermore, a wave function built on the basis of a two-pion exchange three-body force added to the de Tourreil and Sprung interaction (SSCW) is now available¹¹⁻¹³; such a wave function yields an increased binding energy for tritons as is seen in Table II.

Let us mention a few features of the neutron-deuteron scattering state at zero-energy worked out by the theoretical group of Grenoble.² As for the ground state, the Faddeev amplitude has been projected upon five components for the $\frac{1}{2}^+$ state, and seven components for the $\frac{3}{2}^+$ state. The same set of nucleon-nucleon forces has been used, including the SSCW force. In the quartet case $(n+d)_{3/2^+}$, the calculated scattering length $a_{3/2}$ corresponds to the experimental result. The case of the doublet case $(n+d)_{1/2^+}$ is more instructive, since the replacement of SSC by SSCW moves the scattering length $a_{1/2}$ from 1.2 fm to the experimental value 0.65 fm. The correspondence between the triton binding energy and the corresponding scattering length $a_{1/2}$ has been pointed out by Philipps.⁷ Thus, in-

clusion of the three-body force pulls the theoretical values of the scattering length $a_{1/2}$ and the triton binding energy E_T toward their experimental values.²⁻¹³

IV. STATIC MAGNETIC MOMENTS

We are well aware of the existence of several published results on the matter of magnetic moments of $A=3$ ground states; indeed, the following results are meant to compare observables obtained within the framework of Grenoble wave functions with previously established results.

Within the NOIA framework, the following expressions for isovector and isoscalar M 1 moments are well known:

$$\mu_{\text{NOIA}}^s = \frac{1+K_s}{2} (P_S + P_{S'} - P_D) + \frac{P_D}{2}, \quad (5)$$

$$\mu_{\text{NOIA}}^v = \frac{1+K_v}{2} (P_S - \frac{1}{3}P_{S'} + \frac{1}{3}P_D) - \frac{1}{6}P_D, \quad (6)$$

$$\mu^{s,v} = \mu_{\text{NOIA}}^{s,v} + \mu_{\text{MEC}}^{s,v}, \quad (7)$$

where P_S , $P_{S'}$, and P_D , respectively, are the percentage of the completely space symmetric $L=0$ state, mixed space symmetry $L=0$ state, and $L=2$ state.

In the three-body formalism, the MEC contribution takes the following form:

$$\begin{aligned} \langle \Psi_{\text{Tr}} | \vec{M}_{2,3}^{[2]} | \Psi_{\text{Tr}} \rangle &= \sum_{\lambda j} \sum_{\substack{l\sigma J \\ l'\sigma' J'}} \langle \lambda j l \sigma J; \frac{1}{2} | \vec{O}_{23} | \lambda j l' \sigma' J'; \frac{1}{2} \rangle \\ &\times \langle \eta_{(1/2)T}^{1/2-1/2} | O_{23}^T | \eta_{(1/2)T}^{1/2-1/2} \rangle \int \phi_{\lambda j l \sigma J}^{1/2}(x, y) O_{23}(x) \phi_{\lambda j l' \sigma' J'}^{1/2}(x, y) dx dy. \end{aligned} \quad (8)$$

One then defines the transition correlation functions

$$F_{l\sigma Jt; l'\sigma' J't'}^{(1/2)(1/2)}(x) = (-1)^{1+J'} \sqrt{2} \frac{1}{2} \sum_{\lambda j} (-1)^{j+1/2} \begin{Bmatrix} J & 1 & J' \\ \frac{1}{2} & j & \frac{1}{2} \end{Bmatrix} \int \phi_{\lambda l\sigma t}^{j(1/2)(1/2)}(x,y) \phi_{\lambda' l'\sigma' t'}^{j(1/2)(1/2)}(x,y) dy \quad (9)$$

which reduces to the probability density for finding two particles at distance x in the relative states $^{2\sigma+1}l_j$ when the two sets of lowest indices $\{l\sigma JT\}$ and $\{l'\sigma' J'T'\}$ are equal.

Together with such a transition correlation function, the function expressing the transition correlation weighted by the interaction is

$$G_{l\sigma Jt; l'\sigma' J't'}^{(1/2)(1/2)}(x) = F_{\lambda\sigma Jt; l'\sigma' J't'}^{(1/2)(1/2)}(x) O_{23}(x) \langle l\sigma J | \vec{O}_{23} | l'\sigma' J' \rangle \langle \eta_{(1/2)t}^{1/2-1/2} | O_{23}^T | \eta_{(1/2)t'}^{1/2-1/2} \rangle. \quad (10)$$

Table I reproduces the contributions to reduced matrix elements $\langle {}^3\text{H} | \vec{M}^{(1)} | {}^3\text{H} \rangle$ and $\langle {}^3\text{H} | \vec{M}^{(2)} | {}^3\text{H} \rangle$ for the RSC potential. A comparison of the present calculations with the work of Harper *et al.* (HKTR) shows an overall agreement.¹⁴ More specifically, agreement is quite satisfactory for pionic, pair, and N^* diagrams [Figs. 2(a)–(c)] and also for ω - π diagrams [Fig. 2(e)] if one considers that our constant $g_{\omega\pi\gamma}$ is three times larger than theirs. Furthermore, we check that the contributions of the (pair+pionic) diagrams for SS and SD transitions [what HKTR call $\mu_v^{(2)}(X,SS)$ and $\mu_v^{(2)}(X,SD)$] are, respectively, in agreement with the values of HKTR: 0.336 vs 0.338 and 0.264 vs 0.257. Finally, the structure leading to the values 0.336 and 0.264 is somewhat characteristic; for

1S_0 - 3S_1 correlations, the pionic and pair diagrams are individually significant but act with opposite signs ($-0.276+0.612=0.336$), while for 1S_0 - 3D_1 correlations, those same diagrams are individually significantly smaller but add up ($0.132+0.132=0.264$) and then give a comparable contribution. Such an interplay between numbers is also noticeable for the same matrix elements in Table IV of Gari and Huffman.⁶

V. RADIATIVE NEUTRON CAPTURE

The total cross section is a sum of two terms corresponding, respectively, to doublet and quartet states for the scattering n-d state:

$$\sigma = 2 \frac{E_\gamma^3}{\hbar^4 c_j^3} (| \langle \Psi_{3\text{H}}^{1/2} | \vec{M} | \Psi_{n-d}^{1/2} \rangle |^2 + | \langle \Psi_{3\text{H}}^{3/2} | \vec{M} | \Psi_{n-d}^{3/2} \rangle |^2) \frac{1}{9} = \sigma_2 + \sigma_4. \quad (11)$$

The NOIA and MEC operators are identical to those involved in the calculation of the magnetic moments which involve diagonal matrix elements between ground states. Then, in the three-body formalism, one gets expressions very similar to those written for the static magnetic moments, the neutron-deuteron wave function ψ_{n-d} replacing $\psi_{3\text{H}}^{1/2}$.

Within the NOIA framework expressions for transition matrix elements between $(n+d)$, $(\frac{1}{2}^+)$, and ${}^3\text{H}$ are still given by expressions (5) and (6), with $\mathcal{P}_S + \mathcal{P}_{S'} + \mathcal{P}_D = 0$ with

$$\mathcal{P}_S = \int \psi_{(n+d)_{S'}^{1/2}} + \psi_S({}^3\text{H}) \simeq 0,$$

$\psi_S({}^3\text{H})$ being a sum of rather large components; such a situation¹² leads to somewhat delicate estimates of integrals. Replacing \mathcal{P}_S by $\mathcal{P}_{S'} - \mathcal{P}_D$ in Eqs. (5) and (6) expresses NOIA transition matrix elements as functions of $\mathcal{P}_{S'}$ and \mathcal{P}_D which become fundamental quantities. This leads us to assume a bit of inaccuracy in NOIA expressions ($\approx 5\%$).

Table II displays numbers for the various cross sections

carried out in our calculations together with previously published results.^{7,8} Four sets of results linked to the nucleon-nucleon interactions already used in the present article are presented. Furthermore, a column of results originating from an extrapolation explicated later is included under the label Extrapolated. In that table, lines correspond to, respectively,

$$\sigma_2[(n+d)_{1/2}^+ \rightarrow {}^3\text{H} + \gamma],$$

$$\sigma_4[(n+d)_{3/2}^+ \rightarrow {}^3\text{H} + \gamma],$$

$$\sigma_T = \sigma_2 + \sigma_4,$$

and the corresponding percentages of S' and D components in the triton. As far as our own calculations are concerned, columns are ordered in such a way that the binding energies E_T attached to each nucleon-nucleon force increase while going from right to left. Besides the special case of $MT13$ briefly commented on in Fig. 3(a), interesting features come out of reading the NOIA contributions, to wit, the decrease of σ_2 and σ_4 along with the increase of the ${}^3\text{H}$ binding energy and the addition of a three-body force. Those interrelations between σ_2

TABLE I. Reduced matrix elements for single particle and MEC magnetic operators. Note that in the original reference (HKTR, Ref. 14), numbers are given for nonreduced matrix elements.

	$\mu_{\text{isov}}^{(1)}$	$\mu_{\text{isosc}}^{(1)}$	$\mu_{\text{isov}}^{N^*-\pi}$	$\mu_{\text{isov}}^{\omega-\pi}$	$\mu_{\text{isov}}^{\pi+\text{pair}}$	$\mu_{\text{isov}}^{\rho-\pi}$	$\mu_{\text{MEC}}^{3\text{H}}$
HKTR (Ref. 14)	5.272	0.999	0.407	0.029	0.590	0.024	1.05
This work	5.165	0.975	0.430	0.091	0.603	0.031	1.16

TABLE II. The cross sections σ_2 , σ_4 , and σ_T (explained in the text) are given in mb. For each case, two numbers are displayed, separated by commas. The NOIA result is first and the NOIA + MEC result is second.

	Philipps	Hadjimichael	E_{3H} (MeV)				
			-8.6 MT13	-8.48 Extrapolated	-8.17 SSCW	-7.53 SSC	-7.1 RSC
σ_2	0.09,0.50	0.12,0.36	0.166,0.299	0.101,0.488	0.117,0.522	0.150,0.591	0.172,0.649
σ_4	0.064,0.044	0.17,0.16	0.117,0.109	0.124,0.098	0.141,0.113	0.193,0.158	0.267,0.220
σ_T	0.15,0.55	0.29,0.52	0.283,0.408	0.225,0.586	0.258,0.635	0.343,0.748	0.439,0.869
$P_S(^3H)$	1.06	1.6	2.02		1.12	1.35	1.60
$P_D(^3H)$	0	8.0	0		8.5	7.9	9.3

(NOIA), σ_4 (NOIA) and the related reduced matrix element, and E_T are shown in Figs. 3(a), 3(b), and 4. Consideration of these curves led to inclusion of the column labeled Extrapolated; numbers in this column are based on σ_2 (NOIA) and σ_4 (NOIA) extrapolated from calculated

points to the value corresponding to the experimental triton binding energy $E_T = -8.48$ MeV.

MEC contributions are described by the following reduced matrix elements:

$$\langle \Psi_{3H}^{1/2} | \vec{M}_{23}^{[2]} | \Psi_{n-d} \rangle = \sum \sum \langle \lambda j l \sigma J; \frac{1}{2} | \vec{O}_{23} | \lambda j l' \sigma' J'; \frac{1}{2} \rangle \times \langle \eta_{(1/2)l}^{1/2-1/2} | O_{23}^T | \eta_{(1/2)l'}^{1/2-1/2} \rangle \int \phi_{\lambda j l \sigma J}^{1/2}(x, y) O_{23}(x) \Psi_{\lambda j l' \sigma' J'}^{1/2}(x, y) dx dy. \quad (12)$$

One then defines the correlation functions:

$$F_{l\sigma J l' \sigma' J'}^{(1/2)}(x) = (-1)^{1+l'} \sqrt{2} \sum_{\lambda j} (-1)^{j+1/2} \begin{Bmatrix} J & 1 & J' \\ \mathcal{F}' & j & \frac{1}{2} \end{Bmatrix} \int \phi_{\lambda j l \sigma J}^{1/2}(x, y) \Psi_{\lambda j l' \sigma' J'}^{1/2}(x, y) dy, \quad (13)$$

$$\mathcal{F}_{l\sigma J l' \sigma' J'}(x) = F_{l\sigma J l' \sigma' J'}^{(1/2)}(x) O_{23}(x) \langle l \sigma J | \vec{O}_{23} | l' \sigma' J' \rangle \langle \eta_{(1/2)l}^{1/2-1/2} | O_{23}^T | \eta_{(1/2)l'}^{1/2-1/2} \rangle. \quad (14)$$

States which have been considered to describe the scattering state in terms of angular momentum are $\{^{2\sigma+1}l_j\}$ with $l=0,1,2$, $\sigma=0,1$, and $J=0,1,2$ just as for the bound state case. Thus, diagram contributions have been calculated for 22 two-body transitions $\{^{2\sigma+1}l_j \rightarrow ^{2\sigma'+1}l'_j\}$. Table III displays a partial list of

numbers originated from the SSC nucleon-nucleon interaction; quantities corresponding to reduced matrix elements smaller than $0.100 \text{ fm}^{-3/2}$ have been omitted in order to lighten the presentation. Thus, only the four transitions $^1S_0 \leftrightarrow ^3S_1$ and $^1S_0 \leftrightarrow ^3D_1$ give rise to sizable contributions and D - D transitions play no significant role in this problem.

As verified in Table II MEC contributions are quite important especially in the doublet case and are not modified by the incorporation of a three-body force. As for magnetic moments, pionic and pair diagrams contribute in both $^1S_0 \leftrightarrow ^3S_1$ and $^1S_0 \leftrightarrow ^3D_1$ correlations; furthermore, $N^* \pi$ contribution via $^1S_0 \leftrightarrow ^3D_1$ transitions is quite significant. At this stage, it is worth mentioning that the generation of a D state for the n - d continuum leads to fat MEC contributions related to the $^3D_1 \rightarrow ^1S_0$ transitions; such contributions were ignored in previous works.⁷

Before concluding this section, it might be amusing to

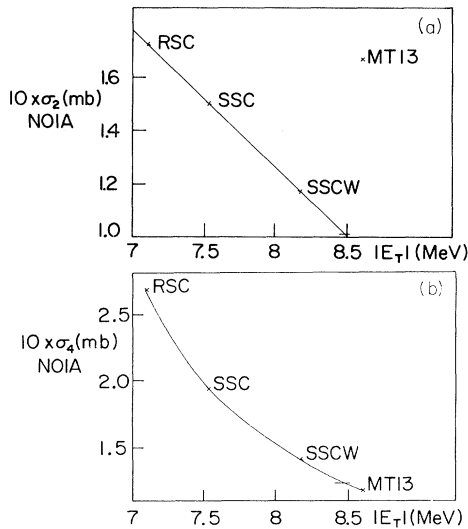


FIG. 3. (a) σ_2 (mb) vs E_{3H} for RSC, SSC, SSCW, and MT13 nucleon-nucleon potentials. As mentioned in the text, P_D is quite important in this particular transition. MT13, having no D state, has a singular behavior. (b) σ_4 (NOIA) vs E_{3H} .

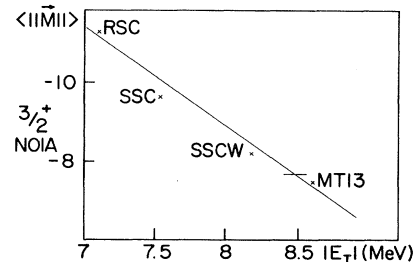


FIG. 4. Reduced matrix element versus E_{3H} in the triplet case for the same potentials as in Fig. 3(b).

TABLE III. Reduced matrix elements of two-body operations ($\text{fm}^{3/2}$) in the case of SSC and σ_2 ($n+d \rightarrow {}^3\text{H} + \gamma$). Quantities lower than 0.100 have been omitted in order to lighten the presentation. Thus, both line and column totals are slightly at variance with written numbers.

Correlations	$\pi-\pi$	$\text{NN}-\pi$	$\text{N}^*-\pi$	$\rho-\rho$	$\text{NN}-\rho$	$\text{N}^*-\rho$	$\text{NN}-\omega$	$\rho-\pi$	$\omega-\pi$	Total
${}^1S_0-{}^3S_1$	-1.286	2.333			0.167					1.356
${}^3S_1-{}^1S_0$	-1.614	2.932			0.209		0.109			1.703
${}^1S_0-{}^3D_1$	0.438	0.438	1.562			-0.548			0.314	2.264
${}^3S_1-{}^1S_0$	0.551	0.551	1.982			-0.696			0.398	2.861
Total	-1.906	6.276	3.649		0.330	-1.259	0.265		0.885	8.309

exhibit some detailed features of the MEC structure. On the basis of soft pion assumptions, diagrams 2(a) ($\pi-\pi$) and 2(b) ($\text{NN}-\pi$) are the "safe diagrams" based on general low-energy theorems while 2(d) and 2(e) behave like corrections to these diagrams. Then the diagram 2(c) ($\text{N}^*\pi$) is a model dependent diagram implying not so soft pions, this diagram being corrected by the diagram 2(f) ($\text{N}^*\rho$). Other corrections are 2(f) ($\rho\rho$), 2(g) ($\text{NN}-\rho$), and 2(i) ($\text{NN}-\omega$). Indeed, all these diagrams have been recalculated by us in the case of $n+p \rightarrow d + \gamma$ also; results confirm the previously published results about the almost complete predominance of the three main diagrams 2(a) ($\pi-\pi$), 2(b) ($\text{NN}-\pi$), and 2(c) ($\text{N}^*\pi$).⁶

A detailed investigation of the numbers in Table III unveils some interesting features about the short range behavior of some of the MEC's. Thus, some looks at the influence of the nucleon-nucleon force on the transition matrix elements involving the singlet n-d state are quite instructive. As an illustration, a set of three pairs of figures exhibits interplay between the various MEC's for the ${}^1S_0-{}^3D_1$; Figs. 5(a) and (b) show very clearly that RSC quenches the short range part of the overlap function for $\text{N}^*-\pi$ in a more drastic way than SSC does. However, Figs. 6(a) and (b), exhibiting the same functions for $\text{N}^*-\rho$,

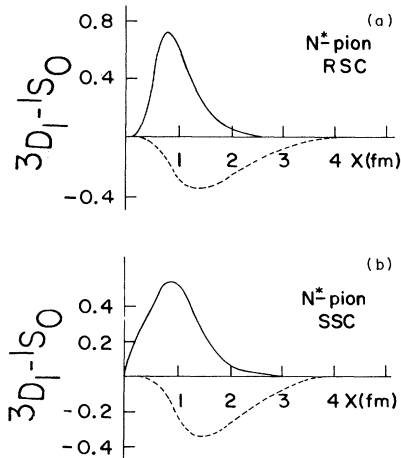


FIG. 5. Two nucleon transition ($\frac{1}{2}^+$) correlation function F and the corresponding function G associated with $\text{N}^*-\pi$, for the ${}^3D_1 \rightleftharpoons {}^1S_0$ transition. F —, G —; (a) corresponds to RSC, (b) corresponds to the SSC nucleon-nucleon force. These conventions are kept for the following figures.

show that this latter current partially cancels the $\text{N}^*-\pi$ contribution at short distance. As a result, and as displayed in Figs. 7(a) and (b), the short range part of the total MEC contribution for ${}^1S_0-{}^3D_1$ correlations is not significantly dependent on the nucleon-nucleon potential.

A different situation holds for the ${}^1S_0-{}^3S_1$ correlations as shown in Figs. 8(a) and (b); in this case, which involves a sum of all diagrams, almost all of the heavy meson contributions are killed by the repulsive effect of the RSC potential while the SSC potential leaves a bump visible at short distance.

It is realized that considerations of the last lines have to do with the short-range domain and hence are of a quite speculative nature. They are, anyway, numerically small; further, a quantitative investigation of this domain most probably requires a new approach based on quarks, with the ${}^3\text{H}$ nucleus considered as a set of three (large or small) bags.

Finally, Table II allows for a comparison of the various theoretical total cross sections σ_T with available experimental values ($0.4 \leq \sigma_T \leq 0.6$ mb). Thus, the RSC nucleon-nucleon force yields a pretty high value for σ_T while the SSC nucleon-nucleon force gives rise to a σ_T closer to its experimental value. The incorporation of a genuine three-body force into SSC makes up for a nucleon-nucleon force that we label SSCW and brings a significant improvement for σ_T ; such a beneficial effect of

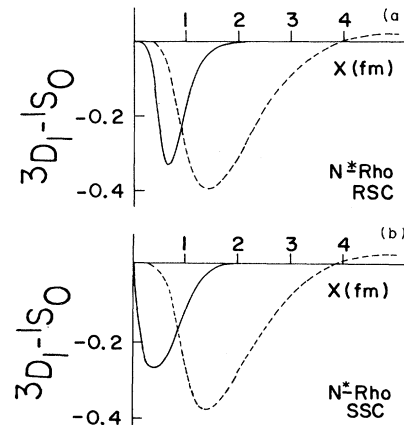


FIG. 6. Two nucleon transition ($\frac{1}{2}^+$) correlation function F and the corresponding function G associated with $\text{N}^*-\rho$, for the ${}^3D_1 \rightarrow {}^1S_0$ transition.

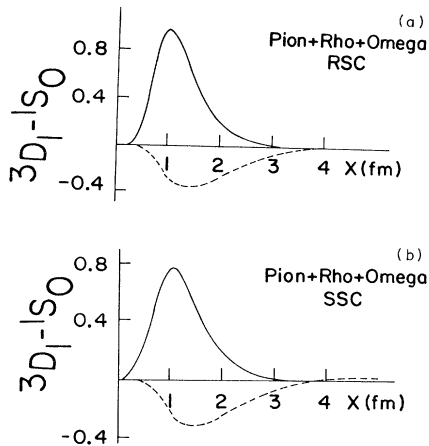


FIG. 7. Two nucleon transition ($\frac{1}{2}^+$) correlation function F and the corresponding function G associated with the sum of all diagrams for the ${}^3D_1 \rightarrow {}^1S_0$ transition.

the incorporation of a genuine three-body force is also present for both the triton binding energy and the neutron-deuteron scattering length $a_{1/2}$. The column labeled "Extrapolated" in Table II, based on extrapolated values of σ_2 and σ_4 which are supposed to correspond to the experimental triton binding energy, yields a total cross section $\sigma_T \approx 0.59$ mb; still closer to the experimental value. Now, one should keep in mind uncertainties attached to the nature of our calculations. As far as NOIA is concerned, the nearly complete orthogonality between the S components of the ${}^3\text{H}$ ground state and of the $(n+d)_{1/2^+}$ scattering state has a bearing on the accuracy of matrix elements roughly estimated at $\approx 5\%$, as already mentioned; due to the lack of a firm theoretical basis, MEC's and especially the $N^*-\pi$ diagram, fairly significant in the present problem, give rise to a 10–20% error so that σ_T is theoretically known within a 15–25% accuracy.

VI. SUMMARY AND CONCLUSION

A calculation of the radiative neutron absorption $n+d \rightarrow {}^3\text{H}+\gamma$ at threshold has been carried out. The enhanced role of MEC's in this process (due to a selection rule acting on the one-body part of the transition matrix element) has been described on the basis of wave functions where a same realistic nucleon-nucleon force gives rise to both the initial zero energy scattering and the final bound state.

These improved wave functions give the opportunity to go beyond the pioneering work of Hadjimichael⁷ on this subject. Thus, the generation of a D state in the neutron-deuteron continuum state leads to ${}^3D_1-{}^1S_0$ MEC contribu-

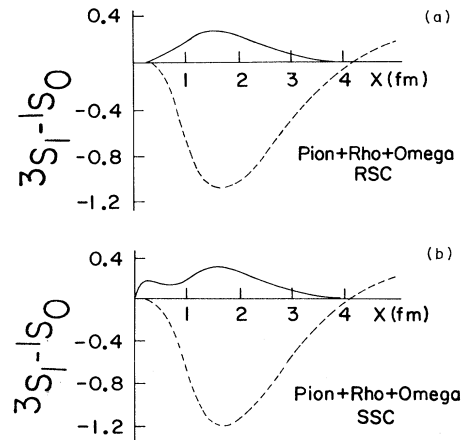


FIG. 8. Two nucleon transition ($\frac{1}{2}^+$) correlation function F and the corresponding function G associated with the sum of all diagrams for the ${}^3S_1 \rightarrow {}^1S_0$ transition.

tions which, absent in Ref. 7, lead to higher values for σ_2 and σ_4 in the present work (Table II). Another new feature of the Grenoble wave function, to wit, a genuine three-body force, tends to compensate for the above-mentioned effect, so that the final number for σ_T in our work, found on the basis of a SSCW nucleon-nucleon force, corresponds to more detailed mechanisms than the value given in Ref. 7.

Our results show specific trends: (i) $\sigma_2(\text{NOIA})$ and $\sqrt{\sigma_4(\text{NOIA})}$ happen to be linear functions of the various triton binding energies corresponding to the nucleon-nucleon forces considered in this work; (ii) MEC contributions are not affected by the inclusion of three-body forces in the case of transition matrix elements; and (iii) inclusion of three-body forces moves $\sigma_2(\text{NOIA})$ toward smaller values while $\sigma_4(\text{NOIA})$ is affected by such three-body forces as well; hence, σ_T moves toward experimental results. The uncertainty of both experimental results ($0.4 \text{ mb} < \sigma_T < 0.6 \text{ mb}$) and theoretical ingredients [the near orthogonality of the S part of the $(n+d)_{1/2^+}$ scattering state and the S part of the triton state makes the NOIA calculation of matrix elements delicate; also the $N^*-\pi$ diagrams are model dependent] is realized. Within such a level of accuracy, the extrapolated value of σ_T ($\sigma_{\text{extrapolated}} \approx 0.59 \text{ mb}$) represents a fairly satisfactory result. It is hoped that the availability of polarized neutron beams and deuteron targets will make it possible to investigate σ_2 and σ_4 on a separate basis, to lead us to an increasingly precise interrelation between experiment and theory.

This work was supported in part by the Natural Sciences and Engineering Council of Canada.

¹A. Laverne and C. Gignoux, Nucl. Phys. **A203**, 597 (1973).

²J. J. Benayoun, C. Gignoux, and J. Chauvin, Phys. Rev. C **23**, 1854 (1981); see also G. L. Payne, J. L. Friar, and B. F. Gibson, *ibid.* **26**, 1385 (1982).

³R. J. Blin-Stoyle, V. Gupta, and H. Primakoff, Nucl. Phys. **11**, 44 (1959).

⁴W. K. Cheng, Ph.D. thesis, University of Pennsylvania, 1966.

⁵M. Chemtob and M. Rho, Nucl. Phys. **A163**, 1 (1971).

- ⁶D. O. Riska and G. E. Brown, Phys. Lett. 38B, 193 (1972); M. Gari and A. H. Huffmann, Phys. Rev. C 7, 994 (1973).
- ⁷E. Hadjimichael, Phys. Rev. Lett. 31, 183 (1973). See also A. C. Phillips, Nucl. Phys. A184, 337 (1972).
- ⁸V. P. Alfimenkov *et al.*, Yad. Fiz. 32, 1491 (1980) [Sov. J. Nucl. Phys. 32, 771 (1980)]. See also recent Los Alamos results $\sigma_T=0.508\pm 0.015$ mb, E. Journey, private communication.
- ⁹G. Konopka, M. Gari, and J. G. Zabolistky, Nucl. Phys. A290, 360 (1977); I. S. Towner and F. C. Khanna, *ibid.* A356, 445 (1981). The constants used in the present paper are essentially the same as those used in this latter reference.
- ¹⁰R. A. Malfliet and J. A. Tjon, Ann. Phys. (N.Y.) 61, 425 (1970).
- ¹¹R. de Turreil, B. Rouben, and D. W. L. Sprung, Nucl. Phys. A242, 44 (1975).
- ¹²R. V. Reid, Ann. Phys. (N.Y.) 50, 441 (1968).
- ¹³J. Torre, J. J. Benayoun, and J. Chauvin, Z. Phys. A 300, 319 (1981).
- ¹⁴E. P. Harper, Y. E. Kim, A. Tubis, and M. Rho, Phys. Lett. 40B, 533 (1972).